

CSI-PPNet: A One-Sided Deep Learning Framework for Massive MIMO CSI Feedback

Wei Chen, *Senior Member, IEEE*, Weixiao Wan, Shiyue Wang, Peng Sun, Bo Ai, *Fellow, IEEE*

Abstract—To reduce multiuser interference and maximize the spectrum efficiency in frequency division duplexing massive multiple-input multiple-output (MIMO) systems, the downlink channel state information (CSI) estimated at the user equipment (UE) is required at the base station (BS). This paper presents a novel method for massive MIMO CSI feedback via a one-sided deep learning framework. The CSI is compressed via linear projections at the UE, and is recovered at the BS using deep plug-and-play priors (PPP). Instead of using handcrafted regularizers for the wireless channel responses, the proposed approach, namely CSI-PPNet, exploits a deep learning (DL) based denoiser in place of the proximal operator of the prior in an alternating optimization scheme. This way, a DL model trained once for denoising can be repurposed for CSI recovery tasks with arbitrary linear projections. In addition to the one-for-all property, in comparison to the two-sided autoencoder-based CSI feedback architecture, the one-sided framework relieves the burden of joint model training and model delivery, and could be applied at UEs with limited device memories and computation power. This opens new perspectives in the field of DL-based CSI feedback. Extensive experiments over the open indoor and urban macro scenarios show the effectiveness of the proposed method.

Index Terms—Massive MIMO, CSI feedback, deep learning, autoencoder, plug-and-play priors.

I. INTRODUCTION

Massive multiple-input multiple-output (MIMO) technology [1] is an essential building block in the fifth-generation (5G) wireless communication system and the 5G-Advanced system. In comparison to the MIMO technology that is used in 4G LTE networks, the increase of the number of antennas improves the network capacity leading to a higher throughput and multi-user support, while it brings new challenges to the design of the communication system, e.g., channel information feedback, pilot signal design, codebook design and beam management [2].

Through three continuous releases of evolution (Rel-15, Rel-16, Rel-17), current 5G protocol supports various scenarios for operations with massive number of antennas [3]–[6]. The major benefit of massive MIMO operation lies in multi-user operation to improve spectral efficiency in addition to improved SINR (signal to interference and noise ratio) for single user operation, considering hardware restrictions in both FR1 and FR2 bands. To realize these promised benefits, current 5G system is based on a flexible protocol framework with support of accurate channel state feedback (including

both channel part and interference part, continuously evolved through three releases with smaller overhead to achieve more accurate channel state information (CSI) feedback), large number of DMRS (Demodulation Reference signal) ports for massive number of users (max 12 orthogonal layers till Rel-17, with the possibility to increase further with pseudo-orthogonal layers), flexible deployment of transmission and reception points (TRP) (single TRP operation, ideal/non-ideal backhaul multiple TRP operations) and various frequency bands for operation with large number of antennas (TDD/FDD bands, FR1/FR2 operation). Currently in Rel-18, the focus of evolving includes aspects from coherent joint transmission operation from multiple TRPs, channel prediction to resolve CSI aging issue, increased number of orthogonal DMRS ports to 24, more diverse operation scenarios with timing difference larger than CP (cyclic prefix) for multiple TRP and etc. [7].

The most efficient massive MIMO techniques require CSI, which can be leveraged to substantially reduce multiuser interference and maximize the spectrum efficiency [2]. In time-division duplexing (TDD) system, the base station (BS) estimates the uplink CSI through the pilot signals transmitted by the user equipment (UE) and then the downlink CSI can be inferred from the uplink CSI by using channel reciprocity. In frequency-division duplex (FDD) system, channel reciprocity is no longer satisfied, as different frequencies are employed in the uplink and downlink. Thus, UEs are required to estimate their own downlink CSI through the local channel estimator, and then feedback the estimated CSI to the BS for subsequent usages. CSI feedback consumes spectrum and energy resources, and the amount of CSI tends to grow with the number of antennas equipped at the BS. Therefore, it is usually desired to feedback a compressed version of the full CSI or features that are sufficient for subsequent usages, e.g., precoding design. In the 5G New Radio (NR) networks, the Type I codebook and the Type II codebook are exploited for CSI feedback. The Type I codebook designed for single-user transmission is relatively simple, but has limited accuracy. The Type II codebook designed for multi-user scheduling has high precision, while the overhead of the Type II codebook is too high to capture fine-grain spatial channel structures in the massive MIMO case [6].

As the massive MIMO channel tends to be sparse owing to the limited local scatters at the BS, various compressive sensing (CS) based CSI compression methods have been studied to address the challenge of overwhelming feedback in massive MIMO systems. The UE takes a reduced number of random measurements of the CSI, and reports the limited measurements to the BS. The original CSI could be recovered

Wei Chen, Weixiao Wan, Shiyue Wang and Bo Ai are with the State Key Laboratory of Rail Traffic Control and Safety, Beijing Jiaotong University, Beijing, China. (e-mail: weich, weixiaowan, shiyuewang, boai@bjtu.edu.cn).

Peng Sun is with vivo Communication Research Institute, Beijing 100015, P.R.China (Email: sunpeng@vivo.com).

by exploiting CS algorithms at the BS. [8] uses CS to reduce the CSI feedback load in a massive-MIMO system by exploiting the expected sparsity in the spatial-frequency domain resulting from spatially-correlated antenna arrays. [9] tackles the massive MIMO CSI feedback using multidimensional CS with the Tucker tensor decomposition, which exploits the channel structure in each dimension (mode) simultaneously. [10] proposes a 1-bit CS-based CSI feedback method, which enables simple and cost-effective construction of the quantizer. [11] compresses channel matrices by using random projection at the UE, and employs deep learning (DL) to recover the original CSI. The classical CS principle leverages the sparse structure of the signal in reconstruction, while the channel matrix is usually not perfectly sparse but nearly sparse. The modeling error in the CS-based CSI feedback methods leads to inevitable CSI reconstruction error.

The state-of-the-art technology for CSI feedback exploits the powerful DL technology that is able to learn non-linear feature representations of the CSI. A DL architecture, named CsiNet [12], uses an encoder to learn a transformation from CSI to codewords at the UE and an inverse transformation to reconstruct the CSI from these codewords at the BS. It is improved into CsiNet+ [13] that exploits the sparsity characteristics of CSI in angular-delay domain, and has a larger receptive field, more refine blocks and deeper network architecture. [14] proposes a fully-convolutional neural network architecture, called DeepCMC, with residual layers at the decoder, and incorporates quantization and entropy coding blocks into its design. DeepCMC is trained to minimize a weighted rate-distortion cost, which enables a trade-off between the CSI quality and its feedback overhead. Beyond the use of convolution layers, there are other effective designs for CSI feedback. Authors in [15] apply long short term memory (LSTM) to extract the temporal correlation of CSI for enhancing recovery performance. Authors in [16], [17] use recurrent neural network (RNN) in both the encoder and decoder to learn temporal correlation. CQNet proposed in [18] is developed to jointly tackle CSI compression, codeword quantization, and recovery under the bandwidth constraint. [19] applies the deep transfer learning to solve the problem of high training cost associated with downlink CSI feedback networks. [20] develops a DL-based CSI feedback framework, which maximizes the beamforming performance gain rather than the feedback accuracy. It should be noted that these DL-based methods follow the idea of source compression and assumes perfect wireless feedback channel that no error occur. Considering the case of imperfect feedback channel, authors in [21] propose a CSI feedback framework based on deep joint source-channel coding (DJSCC), which is superior to the separate source-channel coding scheme and is more robust to the degradation of the feedback channel. Interested readers are referred to [22] for more related work on DL-based CSI feedback.

In most existing DL-based feedback methods [12], [13], [15]–[17], [21], [23]–[27], e.g., CsiNet, CsiNet+ and DJSCC, the DL models at the BS side and the UE side are highly coupled and need to be trained jointly, which leads to several drawbacks. Firstly, the two-sided DL models require collabo-

rations between different network vendors and UE vendors in the training and inference phases, which raises various issues to be considered in order to achieve consensus, e.g., model maintenance and responsibility. Secondly, it is unlikely for UEs to store many DL models due to the limited storage space. For the two-sided DL models, delivering the UE side model from the BS to UEs consumes extra spectrum resource. Thirdly, complex DL models are not suitable for low-cost UEs with limited device memories and computing capability. It is desired to conduct simple operations at the UEs, while the BS can handle computationally intensive tasks.

In this paper, we propose a novel one-sided framework for DL-based CSI feedback. Specifically, the CSI is compressed simply via a small number of linear projections at the UE, and is recovered at the BS in an iterative manner, which involves the use of DL. This method stems from the popular plug-and-play priors (PPP) which was firstly introduced for image reconstruction [28] and then achieved success in many signal processing tasks. The main idea is to unroll the CSI reconstruction problem by variable splitting technique and replace the prior associated subproblem by any off-the-shelf CSI denoising methods. Instead of using handcrafted regularizers for the wireless channel responses, we treat the denoising as a black-box, and capture the angular-delay characteristics existing in the CSI data. Furthermore, the denoise solver can be learned by exploiting DL, which has a large capability in feature abstraction and gives rise to promising performance. We would like to emphasize that the proposed one-sided framework for DL-based CSI feedback is different to those CS-based methods [8], [9], [11], except for the linear projection operation at the UEs. The characteristics of the CSI are learned from data in the proposed work, which avoids enforcing the ideal sparse structure in CS. In addition, we employ the flexible deep PPP [29]–[31] that iteratively applies DL as a denoising operator in the recovery of the CSI at the BS. Deep PPP does not require the knowledge of the process at the UEs in the training phase, and thus is agnostic to the process at the UEs, while the learning based CS network in [11] needs to be trained on a specified projection matrix and cannot be reused for other projection matrices.

The proposed CSI feedback framework has several advantages. Firstly, the DL model at the BS is totally decoupled with operations at the UEs, and is trained without knowing what linear operations are performed to compress the CSI at the UEs. Thus, only the network vendors take the responsibility to maintain the DL model, and the trained DL model can be used for various CSI projection designs of different UE vendors. Secondly, the proposed framework requires the delivery of the projection design from the UE to the BS, which causes light overhead, e.g., only transmitting the random variable seed that generates the random projection matrix. Thirdly, the proposed framework is suitable for UEs with limited device memories and computation power, which conducts linear projections instead of complex DL models.

The rest of the paper is organized as follows: Section II introduces the background and system model of CSI feedback. Section III provides the proposed CSI recovery method, which exploits the deep PPP, and presents details of the network

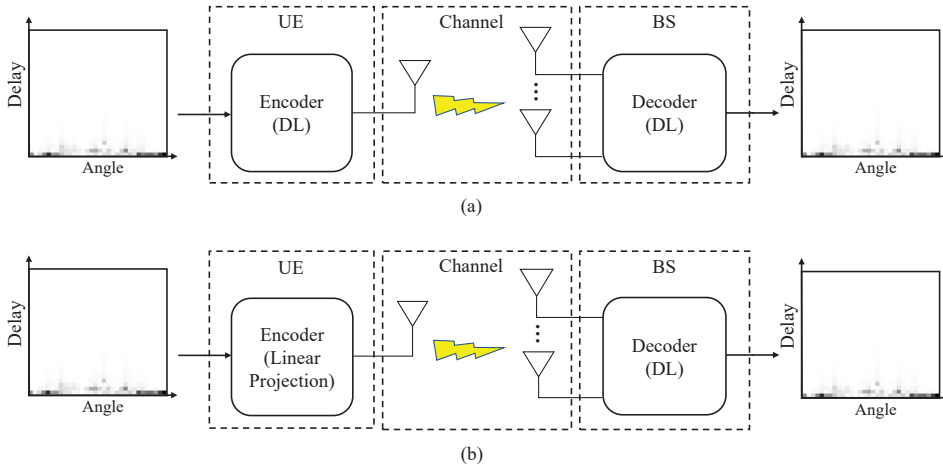


Fig. 1. DL-based CSI feedback frameworks. (a) The two-sided framework, e.g., CsiNet [12], CsiNet+ [13] and DJSCC-Net [21]; (b) The proposed one-sided framework.

architecture and training process. Experimental results are presented in Section IV, followed by conclusions in Section V.

II. SYSTEM MODEL

We consider a single cell massive MIMO orthogonal division multiplexing (OFDM) system operating in the FDD mode. There are N_t antennas equipped at the BS and each UE has a single antenna. Different UEs work at distinct frequency bands. The downlink CSI in the spatial-frequency domain is represented by $\tilde{\mathbf{H}} \in \mathbb{C}^{N_s \times N_t}$, where N_s denotes the number of subcarriers assigned to the UE. In the FDD system, the UE should return $\tilde{\mathbf{H}}$ to the BS through feedback links, and the BS can exploit the CSI to design precoding vectors. In this paper, we assume that perfect CSI has been acquired through pilot-based channel estimation and focus on the design of feedback approaches.

We assume a uniform linear array (ULA) model in the massive MIMO system. To reduce feedback overhead, we could represent the channel matrices in the angular-delay domain using a 2D discrete Fourier transform (DFT), which can be described as following

$$\mathbf{H} = \mathbf{F}_s \tilde{\mathbf{H}} \mathbf{F}_t, \quad (1)$$

where \mathbf{F}_s and \mathbf{F}_t are $N_s \times N_s$ and $N_t \times N_t$ DFT matrices, respectively. The channel matrix in the angular-delay domain contains only a small fraction of large coefficients, and the other coefficients are close to zero. Furthermore, as the time delay between multipath arrivals lies within a limited period, almost all the large coefficients are in the first a few rows of \mathbf{H} in the delay domain. Hence, it is proposed in [11]–[13] to retain the first a few rows of \mathbf{H} for compression at the UE and remove the remaining rows, and then the BS could concatenate the recovered channel matrices with zero rows to obtain full-sized channel matrices. Authors in [21] find that some useful information about the CSI is discarded in the truncation process at the UE, which cannot be compensated in the subsequent process, and suggest to directly compress the full CSI matrices. The proposed methods in this paper

could be applied to both cases, and we use \mathbf{H} to denote the truncated channel matrix by an abuse of notation.

A. The Two-Sided DL-Based CSI Feedback Framework

Most existing DL-based methods for CSI feedback utilize the two-sided autoencoder framework [12], [13], [15]–[17], [21], [23]–[27]. Autoencoder is a type of DL technique used to learn efficient data encodings. The encoder model at the UE maps the CSI matrix to a low-dimensional compressed space, while the decoder model at the BS maps the received feedback information to the original dimension to construct an approximation of the CSI. It naturally overcomes the limits of CS-based approaches that enforce channel sparsity. These existing works mainly focus on the designs of the encoder/decoder DL modules with various considerations, e.g., utilizing more powerful DL building blocks to achieve better performance.

The two-sided DL-based CSI feedback framework is shown in Fig. 1 (a), where the UE-sided model and the BS-sided model could be jointly trained, e.g., at a single side/entity. This leads to a high overhead cost in delivering the DL model from one side to the other side. Separate training at the BS side and UE side requires collaborations, which also results in some sacrifice of communication resources. In addition, the use of DL comes at the considerable cost of computational complexity, which significantly hinders their applications in low-cost UEs, e.g., IoT devices.

B. The One-Sided DL-Based CSI Feedback Framework

The proposed one-sided CSI feedback framework is illustrated in Fig. 1 (b), where only the BS-side requires the deployment of DL models. At the UE, the CSI is simply compressed via a few linear projections which significantly alleviates the burden of computation at the UE. The compression process can be expressed as

$$\mathbf{y} = \mathbf{A}\mathbf{h}, \quad (2)$$

where $\mathbf{h} \in \mathbb{R}^N$ is composed of the real and imaginary parts of the vectored $\tilde{\mathbf{H}} \in \mathbb{C}^{N_s \times N_t}$, $N = 2N_s N_t$, and $\mathbf{y} \in \mathbb{R}^M$

and $\mathbf{A} \in \mathbb{R}^{M \times N}$ denote the compressed CSI vector and the linear projection matrix, respectively. M is the dimension of the feedback CSI, and $\frac{M}{N}$ is the compression ratio. Obviously, M is much less than the dimension of the channel, and thus the feedback overhead is compressed in comparison to the original CSI.

The linear projection matrix \mathbf{A} , which is also called a sensing matrix or a measurement matrix in CS, could be generated randomly. Hence by knowing the random variable seed that is used to generate \mathbf{A} at the UE, the BS could produce the linear projection matrix \mathbf{A} with a negligible amount of communication overhead. The transmission of the random variable seed, e.g., a few bits, is much lighter than the burden of model delivery in the two-sided feedback framework. Although we employ the same process at the UE as CS-based methods [8]–[11], the proposed CSI-PPNet for CSI reconstruction is very different to these existing methods. Firstly, the proposed method exploits a DL model learned directly from CSI training data, which avoids the strict sparse assumption, i.e., the prerequisite of CS-based methods. Secondly, the proposed method offers generalization against various linear projection operations at the UEs, as the model training is agnostic to the compression process. That means the trained DL model at the BS can be applied to arbitrary projection matrices \mathbf{A} for different UEs, and only the network vendors take the responsibility to maintain the DL model.

III. CSI-PPNET

In this section, we present the proposed CSI recovery method, namely CSI-PPNet, which involves a DL model that is agnostic to the process at the UEs.

A. CSI Recovery With the PPP

The recovery of the CSI from compressed feedback in (2) could be boiled down to a Maximum A Posteriori (MAP) estimation problem

$$\hat{\mathbf{h}} = \arg \max_{\mathbf{h}} \log p(\mathbf{y}|\mathbf{h}) + \log p(\mathbf{h}), \quad (3)$$

where $p(\mathbf{y}|\mathbf{h})$ and $p(\mathbf{h})$ denote the likelihood of the feedback \mathbf{y} and the prior of the channel matrix \mathbf{H} , respectively. The MAP estimation problem can be reformulated as

$$\min_{\mathbf{h}} \|\mathbf{y} - \mathbf{A}\mathbf{h}\|_2^2 + \lambda J(\mathbf{h}), \quad (4)$$

where $J(\cdot)$ presents the regularizer incorporating the prior information to enforce the desired delay-angle property of the channel responses, and λ is a positive penalty parameter to control the impact of the regularizer.

There are a few challenges in directly dealing with the CSI recovery problem in (4). Firstly, it is not a trivial task to handcraft an effective regularizer to capture the property of the channel responses. Furthermore, it is not desired to use complex regularizers due to the difficulty of algorithm development. In this paper, we provide a flexible and extendable framework to address this problem, in which any off-the-shelf DL-based denoiser can be exploited.

We first introduce an auxiliary variable \mathbf{z} and the CSI recovery problem (4) can be rewritten as

$$\begin{aligned} \min_{\mathbf{h}, \mathbf{z}} \quad & \|\mathbf{y} - \mathbf{A}\mathbf{z}\|_2^2 + \lambda J(\mathbf{h}) \\ \text{s.t.} \quad & \mathbf{z} = \mathbf{h}. \end{aligned} \quad (5)$$

Various algorithms have been developed to solve this kind of problem. Here, we consider to solve it by minimizing the Lagrangian function

$$L_\rho(\mathbf{h}, \mathbf{z}) = \|\mathbf{y} - \mathbf{A}\mathbf{z}\|_2^2 + \lambda J(\mathbf{h}) + \rho \|\mathbf{h} - \mathbf{z}\|_2^2, \quad (6)$$

where ρ is a positive penalty parameter. By gradually increasing ρ , the solution of (6) tends to be close to the solution of (5). This optimization problem can be addressed by iteratively solving the following subproblems for \mathbf{z} and \mathbf{h} while keeping the rest of the variables fixed,

$$\mathbf{z}^{t+1} := \arg \min_{\mathbf{z}} \|\mathbf{y} - \mathbf{A}\mathbf{z}\|_2^2 + \rho \|\mathbf{h}^t - \mathbf{z}\|_2^2, \quad (7)$$

$$\mathbf{h}^{t+1} := \arg \min_{\mathbf{h}} \lambda J(\mathbf{h}) + \rho \|\mathbf{h} - \mathbf{z}^t\|_2^2. \quad (8)$$

The subproblem in (7) can be solved by the least square method, which gives

$$\mathbf{z}^{t+1} = (\mathbf{A}^T \mathbf{A} + \rho \mathbf{I})^{-1} (\mathbf{A}^T \mathbf{y} + \rho \mathbf{h}^t). \quad (9)$$

The subproblem in (8) can be rewritten as

$$\mathbf{h}^{t+1} := \arg \min_{\mathbf{h}} J(\mathbf{h}) + \frac{\rho}{\lambda} \|\mathbf{h} - \mathbf{z}^t\|_2^2. \quad (10)$$

From a Bayesian perspective, the problem in (10) can be regarded as denoising \mathbf{z}^t in the presence of additive Gaussian noise with a standard deviation $\sqrt{\frac{\lambda}{2\rho}}$ according to the MAP estimation. Instead of handcrafting a regularizer J , we could consider (10) as a denoising problem:

$$\mathbf{h}^{t+1} = \mathcal{D} \left(\mathbf{z}^t, \sqrt{\frac{\lambda}{2\rho}} \right). \quad (11)$$

The denoising process \mathcal{D} captures the delay-angle characteristics of the channel responses. With the various choices of denoising methods, the CSI recovery method is flexible and extendable. The procedure of the proposed CSI Recovery with the PPP is summarized in Algorithm 1.

Solving the subproblem in (8) can be seen as a proximal operation, which is replaced by a denoiser in the PPP method. It is interesting to investigate under which conditions a denoiser can actually be a proximal map, and establish the theoretical convergence of the algorithm. Authors in [32] exploits the theorem of Moreau to prove the convergence of the PPP method, while the analysis is limited to nonexpansive denoisers. Imposing nonexpansiveness to the denoiser is very likely to hurt its denoising performance [33]. Recently, the convergence result is extended to deep denoisers that are not nonexpansive in [34]. In the experimental study, we provide the empirical convergence to show the working mechanism of the proposed deep PPP for CSI recovery.

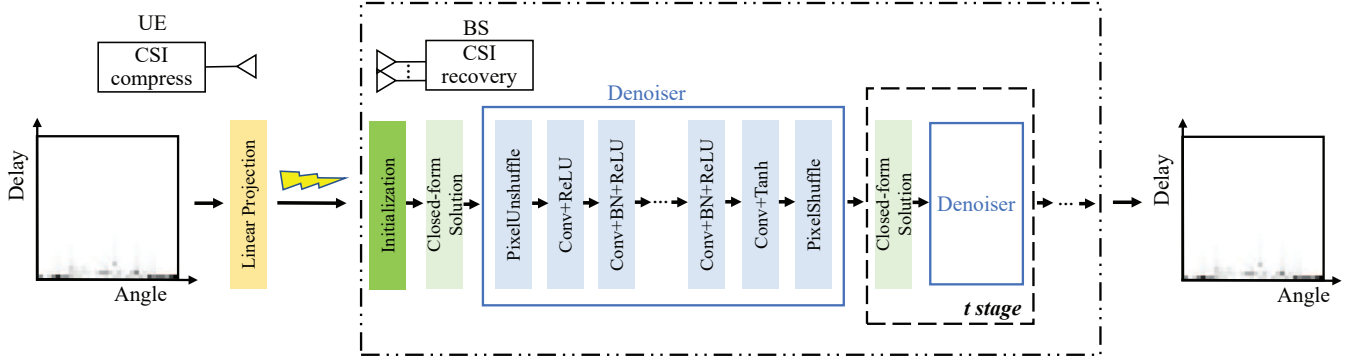


Fig. 2. The proposed one-sided framework with CSI-PPPNet.

Algorithm 1 The proposed CSI Recovery with the PPP

Input: The feedback \mathbf{y} , the linear projection matrix \mathbf{A} , the regularization parameter λ , the penalty factor ρ^1 and the scaling factor α .

Output: The recovered CSI vector, $\hat{\mathbf{h}}$;

Step 1: Initialize the CSI variable \mathbf{h}^0 ;

Step 2: Compute \mathbf{z}^{t+1} using (9);

Step 3: Compute \mathbf{h}^{t+1} using (11);

Step 4: Update $\rho^{t+1} = \alpha\rho^t$;

Step 5: Let $t = t+1$, and go to step 2 if some halting condition is not satisfied.

B. Network Architecture and Training

The proposed one-sided framework with the CSI-PPPNet is shown in Fig. 2. At the UE side, we reshape the real and imaginary parts of the normalized CSI matrix \mathbf{H} into a real-valued vector $\mathbf{h} \in \mathbb{R}^N$. Then we apply linear projections on the CSI vector \mathbf{h} to obtain the feedback vector $\mathbf{y} \in \mathbb{R}^M$. After the BS obtains the feedback vector \mathbf{y} , the CSI-PPPNet is conducted to map it back to the CSI matrix \mathbf{H} . As described in Algorithm 1 and shown in Fig. 2, the proposed method CSI-PPPNet mainly consists of two parts, i.e., the closed-form solution in (9) and the denoiser, which are performed in an alternating way.

At the beginning, we initialize \mathbf{h} at the BS with a rough CSI estimation. Considering the sparsity of the CSI vector \mathbf{h} , we initialize it through a simple non-iterative process. In specific, we apply the least squares estimation on \mathbf{h} according to the support corresponding to a few largest elements in $\mathbf{A}^T \mathbf{y}$. The initialization is described in Algorithm 2. One could also initialize \mathbf{h} with a vector with all zeros, while more iterations are usually needed to achieve good recovery results.

The design of the denoiser module is critical. On the one hand, as CSI-PPPNet is an iterative algorithm, the denoiser module needs to be computational light without sacrificing much denoising performance. On the other hand, as the recovery error of the CSI would gradually decrease in iterations, the denoiser needs to have the ability to adapt to a varying noise variance. With the development of DL technologies, convolutional neural network (CNN) based image denoisers

such as DnCNN [35], IRCNN [36], and FDDNet [37] have shown excellent performance in terms of denoising effectiveness and denoising efficiency. If using the DnCNN, we need to train models for each noise level separately in order to ensure the effectiveness of CSI-PPPNet, which requires huge storage space and training efforts. IRCNN consists of 25 independent 7-layer denoisers, each of which is trained at noise levels within a small range, so that it can handle a range of noise levels. However, this training strategy also lacks flexibility to handle arbitrary noise levels. Different from the DnCNN and the IRCNN, the inputs of the FDDNet are four sub-images generated by downsampling the original noisy image, and a noise level map generated by an adjustable parameter σ . The outputs of the FDDNet are four denoised sub-images, which forms the whole denoised image via reversible upsampling. This unique design allows the network to be guided by the noise level, which makes the network highly adaptable to a varying noise level. In addition, denoising on sub-images improves the network receptive field without increasing the network complexity.

The denoiser used in the CSI-PPPNet is shown in Fig. 2. We reshape the noisy CSI vector $\mathbf{z}^t \in \mathbb{R}^N$ into a tensor $\mathbf{Z}^t \in \mathbb{R}^{N_s \times N_t \times 2}$, and then input it to the network. Inspired by the FDDNet, the first layer of the denoiser is the pixel unshuffle [37] layer, which divides the noisy CSI matrix into four sub-tensors of the size $\frac{N_s}{2} \times \frac{N_t}{2} \times 2$. Then we generate a uniform noise level map of the size $\frac{N_s}{2} \times \frac{N_t}{2}$ with all elements being σ , and concatenate the noise level map with the four sub-tensors into a larger tensor $\hat{\mathbf{Z}}^t \in \mathbb{R}^{\frac{N_s}{2} \times \frac{N_t}{2} \times 9}$. Afterwards, the tensor $\hat{\mathbf{Z}}^t$ is fed into a series of 3×3 convolutional layers, each consisting of a specific combination of four operations: convolution (Conv), rectified linear unit (ReLU), batch normalization (BN) and TanHyperbolic (Tanh). Specifically, the first convolutional layer, the middle layer, and the last convolutional layer adopt the combination of ‘‘Conv+ReLU’’, ‘‘Conv+BN+ReLU’’ and ‘‘Conv+Tanh’’, respectively. The convolutional layers use the zero padding to ensure the size of the feature map unchanged after each convolution. The benefit of using BN in the middle layer is twofold. It would make the network converge faster, and the output of the convolutional layer becomes more stable. In the last convolutional layer,

Algorithm 2 Initialization.

Input: The feedback \mathbf{y} , the linear projection matrix \mathbf{A} , the sparsity K ;

Output: Initialized CSI vector, \mathbf{h}^0 ;

Step 1: Find the set Ω that includes indices corresponding to the top K largest elements in $\mathbf{A}^T \mathbf{y}$;

Step 2: Conduct the least squares estimation, $\mathbf{h}_\Omega = \arg \min_{\mathbf{h}_\Omega} \|\mathbf{y} - \mathbf{A}_\Omega \mathbf{h}_\Omega\|_2^2 = (\mathbf{A}_\Omega^T \mathbf{A}_\Omega)^{-1} \mathbf{A}_\Omega^T \mathbf{y}$;

Step 3: Obtain \mathbf{h}^0 with nonzero elements according to \mathbf{h}_Ω .

the tanh function is used to scale values into the range of $[-1, 1]$. Lastly, the pixel shuffle layer is used as a reverse operation of the pixel unshuffle to generate the denoised CSI. Considering the balance between complexity and performance, we set 8 convolutional layers with 48 convolution kernels in each iteration.

Notably, the DL denoiser can be used for different compression ratios. For the training stage, we normalize the original clean CSI \mathbf{H} and then generate the noisy CSI dataset by adding random Gaussian noise of a variety of noise levels. Each training data sample includes the original clean CSI \mathbf{H} , the noisy CSI $\check{\mathbf{H}}$ and the noise level σ . The denoised channel can be expressed as:

$$\hat{\mathbf{H}} = \text{Denoiser}(\check{\mathbf{H}}, \sigma; \Theta), \quad (12)$$

where Θ represents the parameter set of the denoiser, and σ denotes the noise level of the CSI matrix. To learn model parameters from noisy CSI dataset, we use the loss function given by

$$L(\Theta) = \frac{1}{T} \sum_{j=1}^T \frac{\|\mathbf{H}_j - \text{Denoiser}(\check{\mathbf{H}}_j, \sigma_j; \Theta)\|_F^2}{\|\mathbf{H}_j\|_F^2}, \quad (13)$$

where T is the total number of samples in the training set, the subscript j denotes the j th sample in the training set, and $\|\cdot\|_F$ denotes the Frobenius norm.

IV. EXPERIMENTAL RESULTS

In this section, we evaluate the performance of the proposed CSI-PPPNet, i.e., one-sided framework for massive MIMO CSI feedback. The downlink CSI is generated by QuaDRiGa [38] according to the 3rd Generation Partnership Project (3GPP) TR 38.901 [39]. For the evaluation, we consider two scenarios, i.e., open indoor and urban macro (UMa). The center frequency, inter-site distance, the height of BS and the height of UE are 5.2GHz, 20m, 3m and 1.5m for the indoor scenario, and 2.4GHz, 400m, 25m and 1.5m for the UMa scenario, respectively. There are $N_s = 256$ subcarriers in the OFDM system, and following the setting in [12], [13], [15]–[17], [23]–[27], the first $N_s = 32$ rows which contain most non-zero values are truncated for compression. The BS is equipped with $N_t = 32$ antennas, while the UE has one antenna. Both the antennas in the BS and the UE are omnidirectional. Other specific parameters are shown in Table I.

The generated CSI after normalization forms the training dataset for the denoising network and the evaluation dataset

TABLE I
SIMULATION SETTINGS FOR INDOOR AND UMA.

Parameters	Values
Scenarios	Indoor, UMa
BS antenna configurations	32 elements, omnidirectional
UE mobility	3km/h
Bandwidth	10MHz
UT antenna configurations	1 element, omnidirectional
Center Frequency	5.2GHz for Indoor, 2.4GHz for UMa
Carrier Number	256
Inter-site Distance	20m for Indoor, 400m for UMa
BS height	3m for Indoor, 25m for UMa
UE height	1.5m

for the proposed CSI-PPPNet and other competitors. In the training stage of the denoising network, we generate the noisy CSI by adding random Gaussian noise with the signal to noise ratio (SNR) uniformly drawn in the range of $[0, 40]dB$. Each sample includes the original clean CSI, the noisy CSI and the noise level. The training and validation datasets contain 100,000 and 30,000 samples, respectively. We set the batch size to 128. Adam optimizer is first initialized with a learning rate of 10^{-4} . When the loss does not decrease in 20 epochs, the learning rate will be decayed by half. The lower bound of the learning rate is set to 10^{-7} . Then we generate 20,000 clean CSI samples to evaluate the CSI recovery accuracy and the achievable downlink rate for the proposed CSI feedback method and competitors. To generate the linear projection matrix \mathbf{A} , we apply the singular value decomposition to an $N \times N$ random matrix and use the first M singular vectors to form the M rows of \mathbf{A} . The proposed CSI Recovery with the PPP halts after 10 iterations. The regularization parameter λ , the penalty factor ρ and the scaling factor α are fine-tuned for each CSI compression ratio. The difference between the recovered channel matrix $\hat{\mathbf{H}}$ and the original channel matrix \mathbf{H} is quantified by the normalized mean square error (NMSE), which is expressed as

$$\text{NMSE} = \mathbb{E} \left(\frac{\|\hat{\mathbf{H}} - \mathbf{H}\|_F^2}{\|\mathbf{H}\|_F^2} \right). \quad (14)$$

A. Convergence

The proposed CSI-PPPNet implicitly exploits the DL-based denoising operator as the regularizer in (4), which cannot generally be expressed as a proximal mapping. Therefore, the proposed algorithm does not seek the minimization of an explicit objective function. Without some strong assumptions on the denoiser, it is difficult to provide the theoretical convergence guarantee for the PPP based methods.

To better understand the working mechanism of the proposed CSI-PPPNet for CSI recovery, we illustrate the empirical convergence in Fig. 3. Subfigures on the left show the visual results and NMSE results of the closed-form solution \mathbf{z}^t at different iterations for the indoor and the UMa scenarios. As observed, the recovered CSI matrices in the first iteration contains large errors in comparison to the original

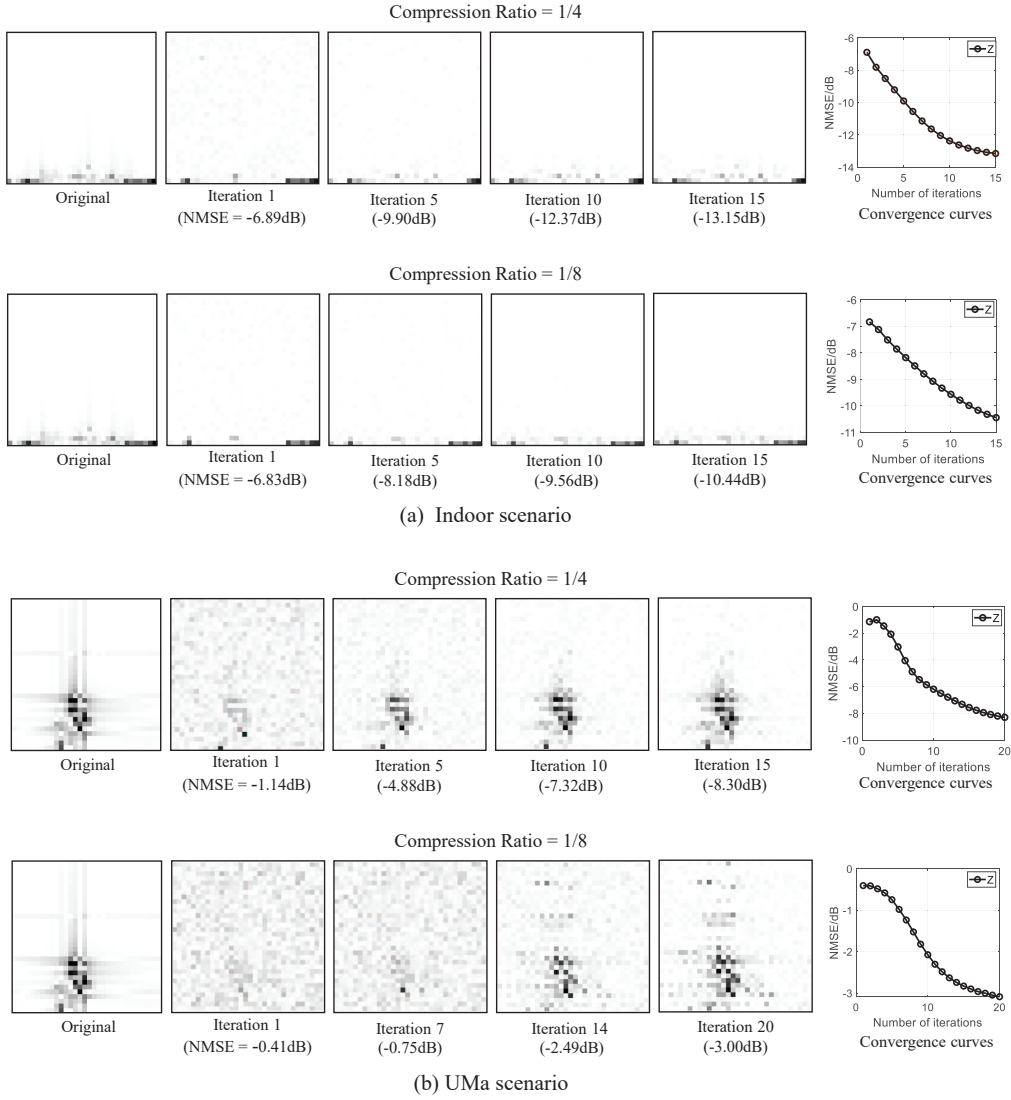


Fig. 3. Illustration of the convergence of the proposed CSI reconstruction method with CSI-PPNet for the indoor and the UMa scenarios. Left: Visual results and NMSE results of the reconstructed CSI matrix at different iterations; Right: Convergence curve of NMSE (y-axis) with respect to the number of iterations (x-axis).

CSI matrices. After passing the results through the DL-based denoiser and updating the closed-form solution several times, the unwanted artifacts are removed and the CSI structures are retained, which results in a decrease of the NMSE. The subfigures on the right show the NMSE convergence curve, from which we can see that the result converge quickly. Note that the NMSE is not guaranteed to decrease with iterations, as we can observe that the NMSE curve of the UMa scenario with the compression ratio 1/4 is not monotonic but it eventually converges.

B. CSI Feedback Accuracy

To evaluate the CSI feedback accuracy, we compare the one-sided CSI-PPNet method with the classical CsiNet, which is a two-sided autoencoder-based method applying DL models at both the UE and the BS. As linear projection is employed by the UE, we also compare the proposed method with TVAL3 [40], i.e., a CS-based algorithm, which is demonstrated

to be superior to several other CS-based algorithms for CSI reconstruction in [11]. In addition to the NMSE that measures the CSI reconstruction error, the cosine similarity (CoS) is another popular CSI feedback accuracy measure used in literature [11]–[13]. As the feedback CSI serves as a beamforming vector, the CoS measures the quality of the beamforming vector, which is given as

$$\text{CoS} = \mathbb{E} \left(\frac{1}{N_s} \sum_{i=1}^{N_s} \frac{|\hat{\mathbf{h}}_i^H \mathbf{h}_i|}{\|\hat{\mathbf{h}}_i\|_2 \|\mathbf{h}_i\|_2} \right), \quad (15)$$

where $\hat{\mathbf{h}}_i$ and \mathbf{h}_i denote the recovered channel vector and the original channel vector of the i th subcarrier, respectively.

Table II and Table III show the CSI feedback accuracy for the indoor scenario and the UMa scenario, respectively. For both scenarios, the proposed method outperforms the CS-based TVAL3 algorithm in terms of the NMSE and the CoS. Its performance is also better than the CsiNet in the UMa scenario

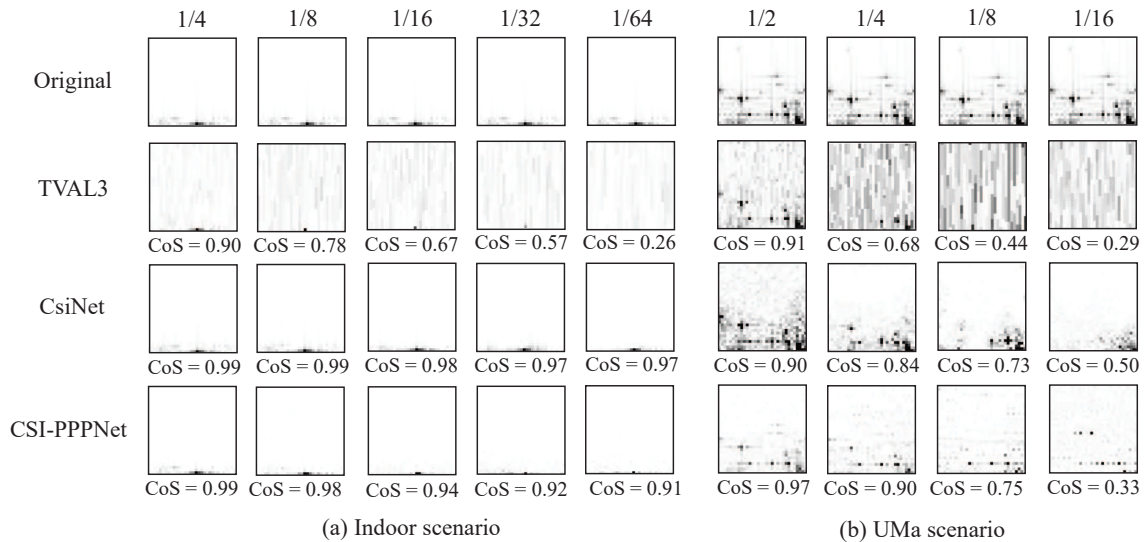


Fig. 4. Visual results comparison of different CSI feedback methods in the indoor scenario and the UMa scenario.

with compression ratios $1/2$ and $1/4$. For the other cases, the CsiNet achieves the highest accuracy. It is not surprising that the two-sided autoencoder-based CsiNet achieves a better CSI feedback accuracy in most cases, as the DL-based encoder at the UE could abstract more compact features than the simple linear projection operation, especially when the compression ratio is low. Therefore, the proposed method can be seen as the result of trading-off the CSI feedback accuracy with the cost in both the encoder complexity and the model training/storage/delivery complexity. In the CSI-PPNet method, a DL model trained once for CSI denoising can be repurposed for CSI recovery tasks with arbitrary linear projections for all UEs. Interestingly, the learning based methods, i.e., the CsiNet and the CSI-PPNet, achieve more accurate CoS than the CS-based TVAL3 algorithm, when their NMSE performance are close. For example, in the indoor scenario, the CSI-PPNet with the compression ratio $1/32$ and the TVAL3 algorithm with the compression ratio $1/8$ achieve similar NMSE, while their CoS are 0.79 and 0.71, respectively. This phenomena suggest the learning based methods would be more promising if considering the construction of beamforming vector using the feedback CSI.

Fig. 4 shows visual results comparison of different CSI feedback methods in the indoor scenario and the UMa scenario. As one can see, the CSI example of the indoor scenario is more sparse than the example of the UMa scenario. Therefore, for all the different methods with the same compression ratio, the CoS performance of the UMa scenario is lower than the performance of the indoor scenario. The TVAL3 method introduces some noticeable false structures, especially when the compression ratio is low. Such odd structures are highly reduced by learning-based methods, i.e., the CsiNet and the CSI-PPNet.

C. Achievable Downlink Rate With CSI Feedback

Furthermore, we consider the achievable downlink transmission rate with CSI feedback in the evaluation. With the

TABLE II
COMPARISON OF THE CSI FEEDBACK ACCURACY FOR THE INDOOR SCENARIO

Compression Ratio	Method	NMSE	CoS
1/4	TVAL3	-10.42	0.90
	CsiNet	-19.16	0.99
	CSI-PPNet	-16.32	0.99
1/8	TVAL3	-3.49	0.71
	CsiNet	-18.12	0.99
	CSI-PPNet	-10.08	0.95
1/16	TVAL3	-1.45	0.55
	CsiNet	-15.88	0.99
	CSI-PPNet	-6.75	0.90
1/32	TVAL3	-0.46	0.35
	CsiNet	-12.78	0.98
	CSI-PPNet	-3.43	0.79
1/64	TVAL3	-0.12	0.21
	CsiNet	-9.48	0.94
	CSI-PPNet	-0.56	0.62

TABLE III
COMPARISON OF THE CSI FEEDBACK ACCURACY FOR THE UMa SCENARIO

Compression Ratio	Method	NMSE	CoS
1/2	TVAL3	-10.05	0.93
	CsiNet	-6.39	0.88
	CSI-PPNet	-11.05	0.96
1/4	TVAL3	-3.90	0.68
	CsiNet	-5.13	0.84
	CSI-PPNet	-6.47	0.89
1/8	TVAL3	-1.77	0.50
	CsiNet	-3.79	0.76
	CSI-PPNet	-2.61	0.73
1/16	TVAL3	-0.59	0.30
	CsiNet	-2.17	0.63
	CSI-PPNet	-0.83	0.48

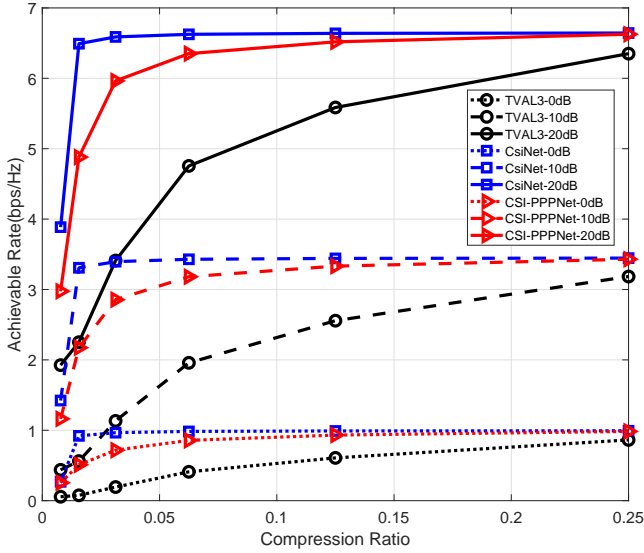


Fig. 5. Comparison of achievable downlink rate with CSI feedback in the indoor scenario.

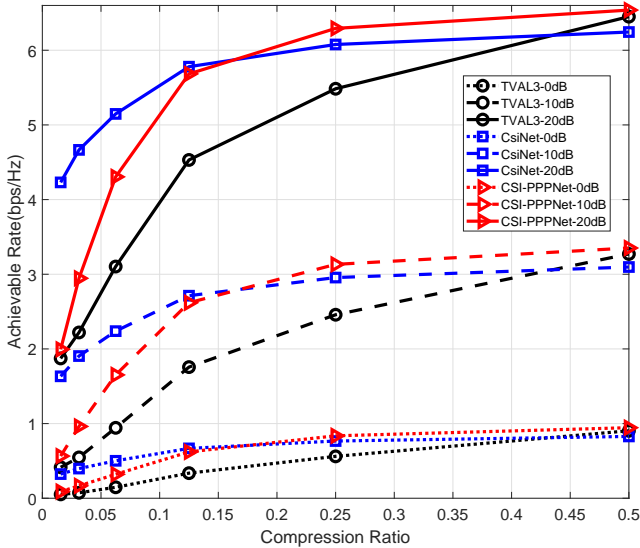


Fig. 6. Comparison of achievable downlink rate with CSI feedback in the UMa scenario.

information of CSI feedback, the BS could use the precoding technology in massive MIMO systems to increasing the throughput. Here, we employ the matched filter (MF) precoding, as it requires low processing complexity. The MF precoding is also known as maximum ratio transmission and conjugate beamforming. The precoding vector for the i th subcarrier is simply the conjugate transpose of the downlink CSI vector, which is given by

$$\mathbf{w}_i = \frac{\hat{\mathbf{h}}_i^H}{\|\hat{\mathbf{h}}_i\|_2}. \quad (16)$$

Then the average achievable downlink rate is

$$R = \mathbb{E} \left(\frac{1}{N_s} \sum_{i=1}^{N_s} \log_2 (1 + \text{SNR}_{DL} |\mathbf{w}_i \mathbf{h}_i|^2) \right), \quad (17)$$

TABLE IV
COMPARISON OF MODEL STORAGE OVERHEAD

Method	UE params	BS params	Total params
CsiNet- $\frac{1}{4}$	1049.3K	1054.7K	2104K
CsiNet- $\frac{1}{8}$	524.7K	530.4K	1055.1K
CsiNet- $\frac{1}{16}$	262.4K	268.2K	530.6K
CsiNet- $\frac{1}{32}$	131.3K	137.1K	268.4K
CsiNet- $\frac{1}{64}$	65.7K	71.6K	137.3K
CsiNet- $\{\frac{1}{4} \cdots \frac{1}{64}\}$	2033.4K	2062K	4095.4K
CSI-PPNet	1	175.2K	175.2K

where SNR_{DL} denotes the downlink SNR. With accurate CSI feedback, we have a larger product between \mathbf{w}_i and \mathbf{h}_i and thus obtain a high achievable downlink rate.

Fig. 5 and Fig. 6 show the achievable downlink rate with CSI feedback in the indoor scenario and the UMa scenario, respectively. Downlink SNRs of 0dB, 10dB and 20dB are considered in the evaluation. The proposed CSI-PPNet achieves the highest achievable downlink rate in the UMa scenario for compression ratio above 0.15. Although the CSINet performs the best for the indoor scenario, the gap between the CSINet and the CSI-PPNet is very small when the compression ratio is larger than 0.1.

D. Model Storage

Now we compare the number of parameters needed in the UE and in the BS to conduct different learning based CSI feedback methods. The number of parameters are given in Table IV. The numbers of parameters are same in both the indoor scenario and UMa scenario, so we do not differentiate the scenarios in presenting the results. The CSINet exploits the autoencoder with an encoder model and a decoder model. The deployment of the DL model imposes extra burden of storage and computation on the UE. Furthermore, as one CSINet model corresponds to a specific CSI compression ratio, several CSINet models corresponding to different compression ratios need to be stored at both the UEs and the BS, if it is desired to adjust the amount of feedback. As shown in Table IV, over 3 million parameters are needed to support CSI compression ratios of $\frac{1}{4}$, $\frac{1}{8}$, $\frac{1}{16}$, $\frac{1}{32}$ and $\frac{1}{64}$ in the CSINet. In comparison, we exploit the one-sided DL framework, where the UE compresses the CSI with a random projection matrix generated by some random variable seed. Thus the UE only needs to store and feedback one extra parameter, i.e., the random variable seed, to the BS. In addition, the CSI-PPNet has an appealing one-for-all property. This means only one DL-based denoiser model needs to be trained and stored at the BS, and is used for arbitrary CSI compression ratios. To support CSI compression ratios of $\frac{1}{4}$, $\frac{1}{8}$, $\frac{1}{16}$, $\frac{1}{32}$ and $\frac{1}{64}$, the proposed method requires no more than 2 hundred thousand parameters in total, which is only 4.3% of the amount of parameters in the CSINet.

V. CONCLUSION

In this work, a novel one-sided DL framework is proposed for massive MIMO CSI feedback. The CSI is compressed via linear projections at the UE, which could be applied at UEs with limited device memories and computation power. Then the CSI is recovered at the BS using DL. We explore the strategy of using the PPP to decouple the DL model training and the UEs' compression procedure, which avoids joint model training and model delivery in traditional two-sided DL models for massive MIMO CSI feedback. The proposed method has an appealing one-for-all property, i.e., one DL-based denoiser model for arbitrary CSI compression ratios, which significantly reduces the number of models for training and storage at the BS. Our experiments show the advantages of the proposed CSI feedback method.

REFERENCES

- [1] E. G. Larsson, O. Edfors, F. Tufvesson, and T. L. Marzetta, "Massive MIMO for next generation wireless systems," *IEEE Communications Magazine*, vol. 52, no. 2, pp. 186–195, 2014.
- [2] L. Sanguinetti, E. Bjornson, and J. Hoydis, "Toward Massive MIMO 2.0: Understanding Spatial Correlation, Interference Suppression, and Pilot Contamination," *IEEE Transactions on Communications*, vol. 68, no. 1, pp. 232–257, 2020.
- [3] 38.211, "NR Physical channels and modulation (Release 17)," *3rd Generation Partnership Project (3GPP), Technical Specification*, 2022.
- [4] 38.212, "NR Multiplexing and channel coding (Release 17)," *3rd Generation Partnership Project (3GPP), Technical Specification*, 2022.
- [5] 38.213, "NR Physical layer procedures for control" (Release 17)," *3rd Generation Partnership Project (3GPP), Technical Specification*, 2022.
- [6] 38.214, "NR Physical layer procedures for data (Release 17)," *3rd Generation Partnership Project (3GPP), Technical Specification*, 2022.
- [7] RP-182863, "MIMO Evolution for Downlink and Uplink," *3rd Generation Partnership Project (3GPP), RAN Meeting 94e*, 2021.
- [8] P.-H. Kuo, H. T. Kung, and P.-A. Ting, "Compressive Sensing Based Channel Feedback Protocols for Spatially-Correlated Massive Antenna Arrays," in *2012 IEEE Wireless Communications and Networking Conference (WCNC)*, 2012, pp. 492–497.
- [9] P. Cheng and Z. Chen, "Multidimensional Compressive Sensing Based Analog CSI Feedback for Massive MIMO-OFDM Systems," in *2014 IEEE 80th Vehicular Technology Conference (VTC2014-Fall)*, 2014, pp. 1–6.
- [10] C. Qing, Q. Yang, B. Cai, B. Pan, and J. Wang, "Superimposed Coding-Based CSI Feedback Using 1-Bit Compressed Sensing," *IEEE Communications Letters*, vol. 24, no. 1, pp. 193–197, 2020.
- [11] P. Liang, J. Fan, W. Shen, Z. Qin, and G. Y. Li, "Deep Learning and Compressive Sensing-Based CSI Feedback in FDD Massive MIMO Systems," *IEEE Transactions on Vehicular Technology*, vol. 69, no. 8, pp. 9217–9222, 2020.
- [12] C.-K. Wen, W.-T. Shih, and S. Jin, "Deep Learning for Massive MIMO CSI Feedback," *IEEE Wireless Communications Letters*, vol. 7, no. 5, pp. 748–751, 2018.
- [13] J. Guo, C.-K. Wen, S. Jin, and G. Y. Li, "Convolutional Neural Network-Based Multiple-Rate Compressive Sensing for Massive MIMO CSI Feedback: Design, Simulation, and Analysis," *IEEE Transactions on Wireless Communications*, vol. 19, no. 4, pp. 2827–2840, 2020.
- [14] M. B. Mashhadi, Q. Yang, and D. Gunduz, "Distributed Deep Convolutional Compression for Massive MIMO CSI Feedback," *IEEE Transactions on Wireless Communications*, vol. 20, no. 4, pp. 2621–2633, 2021.
- [15] T. Wang, C.-K. Wen, S. Jin, and G. Y. Li, "Deep Learning-Based CSI Feedback Approach for Time-Varying Massive MIMO Channels," *IEEE Wireless Communications Letters*, vol. 8, no. 2, pp. 416–419, 2019.
- [16] C. Lu, W. Xu, H. Shen, J. Zhu, and K. Wang, "MIMO Channel Information Feedback Using Deep Recurrent Network," *IEEE Communications Letters*, vol. 23, no. 1, pp. 188–191, 2019.
- [17] X. Li and H. Wu, "Spatio-Temporal Representation With Deep Neural Recurrent Network in MIMO CSI Feedback," *IEEE Wireless Communications Letters*, vol. 9, no. 5, pp. 653–657, 2020.
- [18] Z. Liu, L. Zhang, and Z. Ding, "An Efficient Deep Learning Framework for Low Rate Massive MIMO CSI Reporting," *IEEE Transactions on Communications*, vol. 68, no. 8, pp. 4761–4772, 2020.
- [19] J. Zeng, J. Sun, G. Gui, B. Adebisi, T. Ohtsuki, H. Gacanin, and H. Sari, "Downlink CSI Feedback Algorithm With Deep Transfer Learning for FDD Massive MIMO Systems," *IEEE Transactions on Cognitive Communications and Networking*, vol. 7, no. 4, pp. 1253–1265, 2021.
- [20] J. Guo, C.-K. Wen, and S. Jin, "Deep Learning-Based CSI Feedback for Beamforming in Single- and Multi-Cell Massive MIMO Systems," *IEEE Journal on Selected Areas in Communications*, vol. 39, no. 7, pp. 1872–1884, 2021.
- [21] J. Xu, B. Ai, N. Wang, and W. Chen, "Deep Joint Source-Channel Coding for CSI Feedback: An End-to-End Approach," *IEEE Journal on Selected Areas in Communications*, Preprint.
- [22] J. Guo, C.-K. Wen, S. Jin, and G. Y. Li, "Overview of Deep Learning-based CSI Feedback in Massive MIMO Systems," *arXiv preprint arXiv:2206.14383*, 2022.
- [23] Z. Hu, J. Guo, G. Liu, H. Zheng, and J. Xue, "MRFNet: A Deep Learning-Based CSI Feedback Approach of Massive MIMO Systems," *IEEE Communications Letters*, vol. 25, no. 10, pp. 3310–3314, 2021.
- [24] X. Chen, C. Deng, B. Zhou, H. Zhang, G. Yang, and S. Ma, "High-Accuracy CSI Feedback With Super-Resolution Network for Massive MIMO Systems," *IEEE Wireless Communications Letters*, vol. 11, no. 1, pp. 141–145, 2022.
- [25] Z. Cao, W.-T. Shih, J. Guo, C.-K. Wen, and S. Jin, "Lightweight Convolutional Neural Networks for CSI Feedback in Massive MIMO," *IEEE Communications Letters*, vol. 25, no. 8, pp. 2624–2628, 2021.
- [26] S. Ji and M. Li, "CLNet: Complex Input Lightweight Neural Network Designed for Massive MIMO CSI Feedback," *IEEE Wireless Communications Letters*, vol. 10, no. 10, pp. 2318–2322, 2021.
- [27] Z. Lu, J. Wang, and J. Song, "Binary Neural Network Aided CSI Feedback in Massive MIMO System," *IEEE Wireless Communications Letters*, vol. 10, no. 6, pp. 1305–1308, 2021.
- [28] S. V. Venkatakrisnan, C. A. Bouman, and B. Wohlberg, "Plug-and-Play priors for model based reconstruction," in *2013 IEEE Global Conference on Signal and Information Processing*, 2013, pp. 945–948.
- [29] W. Chen, D. Wipf, and M. Rodrigues, "Deep Learning for Linear Inverse Problems Using the Plug-and-Play Priors Framework," in *ICASSP 2021 - 2021 IEEE International Conference on Acoustics, Speech and Signal Processing (ICASSP)*, 2021, pp. 8098–8102.
- [30] K. Zhang, Y. Li, W. Zuo, L. Zhang, L. Van Gool, and R. Timofte, "Plug-and-Play Image Restoration With Deep Denoiser Prior," *IEEE Transactions on Pattern Analysis and Machine Intelligence*, vol. 44, no. 10, pp. 6360–6376, 2022.
- [31] M. Zhao, X. Wang, J. Chen, and W. Chen, "A Plug-and-Play Priors Framework for Hyperspectral Unmixing," *IEEE Transactions on Geoscience and Remote Sensing*, vol. 60, pp. 1–13, 2022.
- [32] S. Sreehari, S. V. Venkatakrisnan, B. Wohlberg, G. T. Buzzard, L. F. Drummy, J. P. Simmons, and C. A. Bouman, "Plug-and-Play Priors for Bright Field Electron Tomography and Sparse Interpolation," *IEEE Transactions on Computational Imaging*, vol. 2, no. 4, pp. 408–423, 2016.
- [33] E. Ryu, J. Liu, S. Wang, X. Chen, Z. Wang, and W. Yin, "Plug-and-play methods provably converge with properly trained denoisers," in *International Conference on Machine Learning*, 2019, pp. 5546–5557.
- [34] S. Hurault, A. Leclaire, and N. Papadakis, "Proximal denoiser for convergent plug-and-play optimization with nonconvex regularization," *arXiv preprint arXiv:2201.13256*, 2022.
- [35] K. Zhang, W. Zuo, Y. Chen, D. Meng, and L. Zhang, "Beyond a gaussian denoiser: Residual learning of deep cnn for image denoising," *IEEE Transactions on Image Processing*, vol. 26, no. 7, pp. 3142–3155, 2017.
- [36] K. Zhang, W. Zuo, S. Gu, and L. Zhang, "Learning Deep CNN Denoiser Prior for Image Restoration," in *2017 IEEE Conference on Computer Vision and Pattern Recognition (CVPR)*, 2017, pp. 2808–2817.
- [37] K. Zhang, W. Zuo, and L. Zhang, "Ffdnet: Toward a fast and flexible solution for cnn-based image denoising," *IEEE Transactions on Image Processing*, vol. 27, no. 9, pp. 4608–4622, 2018.
- [38] S. Jaeckel, L. Raschkowski, K. Borner, and L. Thiele, "QuADRIga-quasi deterministic radio channel generator, user manual and documentation," *Fraunhofer Heinrich Hertz Institute, Tech. Rep. v2.6.1*, 2021.
- [39] 3GPP, "5G; Study on channel model for frequencies from 0.5 to 100 GHz," *3rd Generation Partnership Project (3GPP), Tech. Rep. 38.901 V16.1.0*, 2020.
- [40] C. Li, W. Yin, and Y. Zhang, "User's guide for TVAL3: TV minimization by augmented lagrangian and alternating direction algorithms," [Online]. Available: <http://www.ccam.rice.edu/optimization/LI/TVAL3/>.